



## **Post-buckling strength of single layer domes under distributed loading**

Prahlad Dara<sup>1</sup>, Raghavan Ramalingam<sup>2</sup>, Gorripotu Kishorekumar<sup>3</sup>

### **Abstract**

Global stability is a critical aspect of reticulated shells and may govern the design of these structures. because of the shallow geometry and the large deflection coming from such structures. This global instability might occur in the form of snap-through buckling before even the critical loads of the members are reached. Literature provides approximate theories for calculating these limits, by assuming them as equivalent thin shells and checking the adequacy of members using clauses of design codes for members of the reticulated shells. However this leads to conservative cross-sections as required by codal provisions of member strength and stability, even though the global shell buckling may govern the design of reticulated shells. This shows the need for an accurate prediction of the critical loads of these systems. Inelastic postbuckling analysis by several researchers largely consider apex loading, thus neglecting the distribution of loads across all nodes of the dome, present in actual structures. Thus in order to have a practically usable prediction equation, these distributed loadings need to be considered. This study has uses a geometric non-linear analysis based on a corotated – updated Lagrangian (CR-UL) formulation to predict the behavior of the systems. This study shows that neglecting load distributions is highly inaccurate and on the conservative side. The effect of important geometric parameters on the limit loads are also discussed. The study also attempts a linear regression equation for predicting the limit and ultimate loads of the dome.

### **1. Introduction**

The stability of reticulated domes has been studied extensively for ascertaining with practical precision the critical loads. This has not been achieved satisfactorily not only due to the nonlinear behavior, but also because the extent of influence of each physical parameter is not fully clear. Through reading of available literature to date, the critical factors affecting the stability of these structures can be viewed at three different levels namely – global stability, local (member) strength and stability, and connection idealisations. Indeed the literature present is such that the studies undertaken in them are found to address the effect of one of the above factors. Even the variations present in each of these components has deserved research in isolation to study its effect, e.g., the variations in connection components such as socket joints, plated connectors etc are unique.

---

<sup>1</sup> Postgraduate Student, National Institute of Technology Tiruchirappalli, <prahladdara4567@gmail.com>

<sup>2</sup> Assistant Professor, National Institute of Technology Tiruchirappalli, <raghavanr@nitt.edu>

<sup>3</sup> Graduate Research Scholar, National Institute of Technology Tiruchirappalli, <kishore7142@gmail.com>

Chronology-wise the earliest researchers such as Papadrakakis (1983), Hill et al (1989), Yang et al (1997), Jayachandran et al (2004), Thai and Kim (2009) etc worked on quantifying the effect of member strength and stability on that of the whole structure. Constitutive models for member stress-strain relations and the development of robust solution procedures to overcome the limit points, in particular the works of Argyris et al (1982), Crisfield (1981), Bergen and Soreide (1978), Belytschko and Hsieh (1973), Chan et al (1988) et al. One of the key concerns expressed through all the literature in this period (of the literature referred above) is the absence of a procedure that provides means of estimating the limit loads of the structure, barring general recommendations in some documents such as the working committee report of the International Association of Shell and Spatial Structures (IASS). Recent research has shown a gradual shift towards studying the behavior of different kinds of connections and the performance of the structure with each type of connection. Key literature in this area include those by Lopez et al (2007), Ahmadizadeh and Maleek (2014), Ma et al (2015), Guo et al (2015), Han et al (2016), Xiong et al (2017) etc. The findings of these studies establish that the characteristics of the types of joints have a significant bearing on the limit load of the structure. A key point of mismatch with reality in the majority of the studies is that the analyses are performed for concentrated loads the apex, rather than with loading across the surface as is expected in reality (from wind pressures).

Nowadays the availability of commercial FEM software enables designers to verify the structure against limit point failures. This however does not have the same convenience as calculations using closed form expressions, the oldest of which is the Wright's formula (1965). Lopez et al (2007) and Saito (1986) suggest analyticals expression for obtaining critical pressures of single layer domes. These however are confined to elastic regimes and do not match the nonlinear behavior of domes.

Following the above discussions, the authors of this paper propose the following aims: (a) compare the limit point behavior of single layer domes under two distributed loading patterns with that of apex loading of equivalent magnitude, (b) check the applicability of the Wright's formula for the two loading patterns and (c) propose closed-form equations to obtain the critical load of single layer domes. The above studies are performed on domes of two geometries as discussed below.

## **2. Postbuckling analysis using CR-UL formulation**

For the post-buckling analysis in this study, the corotated-updated Lagrangian (CR-UL) nonlinear formulation is used. The total load-deflection behavior of reticulated shells both before and after limit points like snap-through can be traced using the formulation. The updated Lagrangian formulation uses all quantities in the finite element equations referred to the last known configuration as the reference configuration rather than the original configuration in a total Lagrangian formulation. In the corotated approach, the deformations of the elements are explicitly separated into rigid body displacements and stress producing (natural) deformations. The detailed mathematical explanations and derivations are given in Jayachandran et al (2004).

To make the discussion short, the final equations for obtaining the local and global tangent stiffness are alone listed below.

$$K_L = \frac{A}{L}(C + \sigma) \quad (1)$$

$$K_G = A^T (E^T K_L E + R_{x2} B) A \quad (2)$$

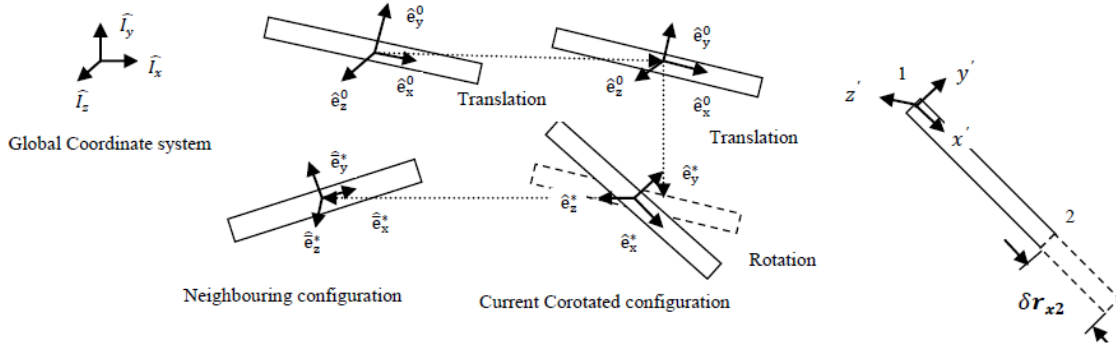


Figure 1: Description of motion in the CR formulation

Here  $C$  is the constitutive matrix,  $\sigma$  is the stress and  $A$  and  $E$  are transformation matrices corresponding to the different configurations in Fig 1. A bilinear hardening formulation (Axelsson and Samuelsson, 1979) is used for incorporating yielding in the members using the state determination procedure (Bhatti, 2006) (Fig. 2 and Eqs. 3-5). Modifications for reduced member stiffness due to buckling is as used by Jayachandran et al (2004) in Eqs. 6-7.

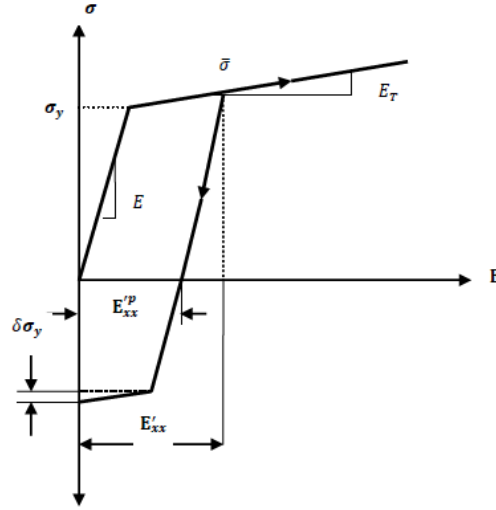


Figure 2: Bilinear stress-strain model with mixed hardening

$$\delta E'_{xx} = (1 - \beta) \delta E'_{xx} \quad (3)$$

$$\delta \sigma_y = MH \delta E'_{xx} \quad (4)$$

$$\delta \alpha = (1 - M) H E'_{xx} \quad (5)$$

$$F_{\Delta} = \left[ 1 - \frac{1}{1 + \frac{2}{3} \left( \frac{\delta_c}{L} \right)^2} \right] \quad (6)$$

$$K'_L = \frac{1}{\left[ \left( \frac{1}{\frac{A}{L}(C+\sigma)} \right) + \frac{F_{\Delta}L}{R_{x2}} \right]} \quad (7)$$

The plastic and total strain increments are  $\delta E'_{xx}$  and  $\delta E'_{xx}$ , and the portion of elastic in total strain increment is  $\beta$ . The changes to the subsequent yield stress and stress shift vectors are given by  $\delta\sigma_y$  and  $\delta\alpha$  in terms of the hardening parameter  $M$  and hardening modulus  $H$ . The reduced member stiffness after buckling  $K'_L$  is in terms of the length  $L$  and midlength deflection  $\delta_c$ . The solution procedure adopted for traversing the limit point is the minimum residual displacement method by Chan (1988). The overall procedure is implemented in a computer program. This program is used to undertake a series of analysis on single-layer domes under different loading patterns. Both elastic and inelastic analyses (i.e., considering member yielding and buckling) can be done separately using the above program.

### 3. Analysis series on single-layer domes with distributed loading patterns/

#### 3.1 Validation example

In order to show the validity of the procedure, the results of analyzing the 168-bar dome present in Thai and Kim (2009) is shown in Fig 3. The load factor is for a reference load of 1000 N. Note that the literature analyses the structure only with apex loading, which matches the results from this formulation. However, performing the analysis on the same structure shows the inherent conservativeness while adopting apex loading conditions for finding limit points, as compared to more practical distributed loading.

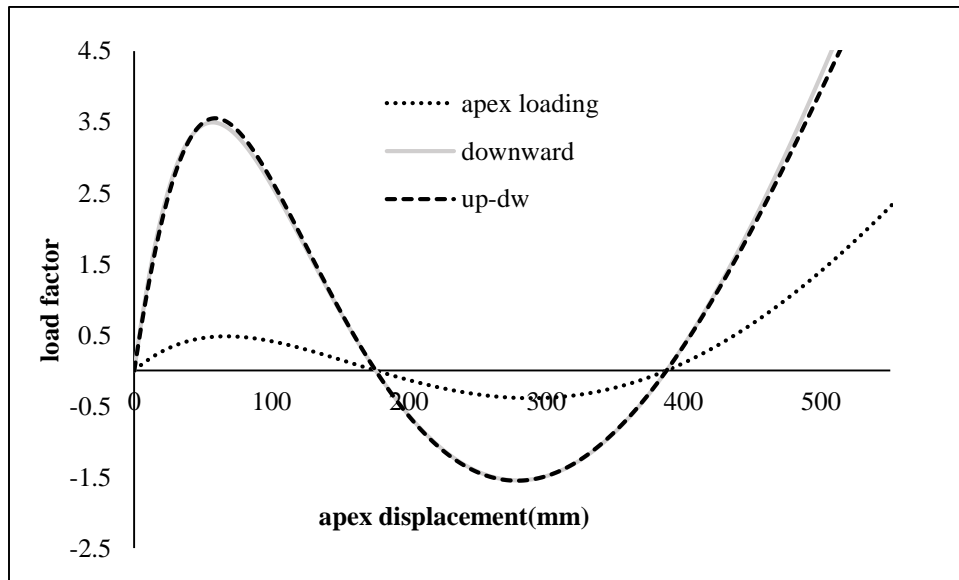


Figure 3: Postbuckling curves of 168-bar dome (Thai and Kim, )

#### 3.2 Geometry and dimensions of domes

Two dome geometry types are studied in this paper. Geometry Type 1 has a uniform arrangement of the members such that all members have same length, similar to but not exactly at Geodesic

dome. Here it shall be called as Geodesic for convenience. Geometry Type 2 is Lamella in which member lengths get longer between lower rings of the dome. These geometries are shown in Fig 4. Since the member rigidities are controlling parameters more than the cross-sectional areas and moment of inertias themselves, the latter are kept same for all examples. The cross-sectional area and moment of inertia correspond to a steel tube of 80 mm diameter and 5.72 mm thickness having Modulus of Elasticity  $2.1 \times 10^8$  kN/m<sup>2</sup>. All other properties of the dome varied for the study are shown in Table 1 and Table 2. For convenience, the final calculated average values of the axial and flexural rigidities are also shown in the table. The reference load for all examples amounts to 100 kN, which is applied as a point load downward at the apex. For distributed loading patterns, two conditions are adopted, one with downward (pressure) loading at all the nodes, and one with pressure loading on one half and uplift on the other (with loading downward at the apex). For both distributed loading conditions, 40 kN downward load is applied at the top while the balance 60 kN is distributed equally at all rings. For example, if a dome had 3 rings (excluding at support level), the remaining two rings will carry a total of 30 kN each, and if there were 16 nodes on the ring, each node would carry 1.875 kN. These are depicted in Fig 5. This distribution of the load in the half pressure-half uplift case is close to adopting external wind pressure coefficients of +0.3 for windward quarter, +0.4 for central portion and -0.3 for the leeward quarter.

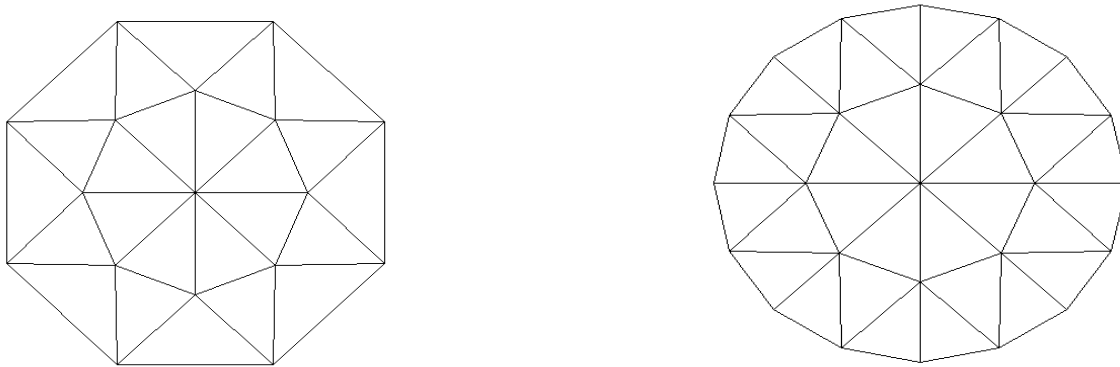


Figure 4: Geometry of Lamella Type dome (left) and Geodesic Type dome (right)

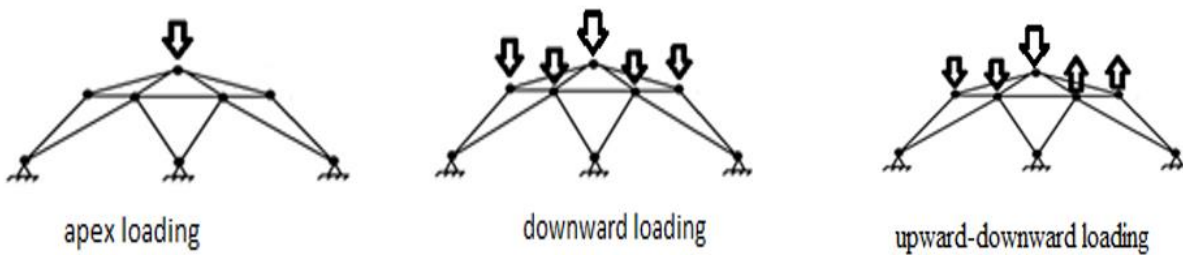


Figure 5: Loading distribution patterns on the domes

### 3.3 Discussion of results

The postbuckling curve for one example of the geodesic dome is shown in Fig 6 and Fig 7 for elastic and inelastic analysis runs. It is seen in this example that, in both cases the limit loads predicted with applying distributed loads is around 2.6-2.7 times that obtained by loading only the

apex. The inelastic analysis plot also gives information on the ultimate loads of the dome i.e the point beyond which the solution increments fail to converge due to buckling of a group of members (the final point of the graph) or when yielding of a group of members takes place. In Fig 7, since the ultimate load point was by buckling of members, the final point of the graph is taken as the ultimate load. In the half pressure-half uplift case, the solution diverges before the plot resumes positive trend and hence the ultimate load point was not determined. This happened for most of the examples with half pressure-half uplift loading.

Table 1: Properties of Geodesic type domes (units: kN, m)

S.No	Dome model	Span/Rise	Rings	Members at apex	AE/L	EI/L
1.	Geodesic 1	5	2	8	53532.6	48.52
2.	Geodesic 2	6	2	8	37698.5	34.17
3.	Geodesic 3	5	2	12	54576.5	49.47
4.	Geodesic 4	4	2	16	58749	53.25
5.	Geodesic 5	8	3	12	25049.1	22.70
6.	Geodesic 6	8	3	8	21373.3	19.37
7.	Geodesic 7	8	3	16	28087.8	25.46
8.	Geodesic 8	8	4	12	50188.9	45.49
9.	Geodesic 9	8	4	8	36019	32.65
10.	Geodesic11	10	2	8	14735.9	13.36
11.	Geodesic12	10	2	12	17157.3	15.55
12.	Geodesic13	10	2	16	18553.9	16.82
13.	Geodesic14	10	3	8	21648.6	19.62
14.	Geodesic15	10	3	12	25121	22.77
15.	Geodesic16	10	3	16	27218.4	24.67
16.	Geodesic17	10	4	8	28665.6	25.98
17.	Geodesic18	10	4	12	33216.8	30.11
18.	Geodesic19	10	4	16	35942.3	32.58
19.	Geodesic20	8	2	8	14541	13.18
20.	Geodesic21	8	2	12	16939.6	15.35
21.	Geodesic22	8	2	16	18383.6	16.66
22.	Geodesic23	8	3	8	21433.5	19.43
23.	Geodesic24	8	3	12	24809.7	22.49
24.	Geodesic25	8	3	16	26905	24.39
25.	Geodesic26	8	4	8	28318.2	25.67
26.	Geodesic27	8	4	12	32827.9	29.75
27.	Geodesic28	8	4	16	35487.3	32.16
28.	Geodesic29	6	2	8	18981	17.20
29.	Geodesic30	6	2	12	22074.8	20.01
30.	Geodesic31	6	2	16	23900.3	21.66
31.	Geodesic32	6	3	8	27923.3	25.31
32.	Geodesic33	6	3	12	32373	29.34
33.	Geodesic34	6	3	16	34982.5	31.71
34.	Geodesic35	6	4	8	36888.2	33.43
35.	Geodesic36	6	4	12	42736.3	38.73
36.	Geodesic37	6	4	16	46186.2	41.86

The above can be explained by the sign of the forces in the members. When the loading is entirely pressure or only at apex, all the ring members are under tension till the plot resumes positive trend after the snap-through (while radial members are under compression which buckle causing the first limit point). With half pressure-half uplift loading, some of the ring members are already in compression before the resumption of the positive trend. The ultimate failure, is thus predicted at

this point, since member buckling has occurred in both ring and radial members simultaneously. This could have implications on member selection for ring and radial members when designing for such a load distribution, which is commonly encountered for wind pressures on the surfaces of dome.

Table 2: Properties of Lamella type domes (units: kN, m)

S.No	Dome model	Span/Rise	Rings	Members at apex	AE/L	EI/L
1.	Lamella1	5	2	8	37885.1	34.34
2.	Lamella2	5	2	8	32076.7	29.07
3.	Lamella3	5	2	12	44387.3	40.23
4.	Lamella4	6	2	10	37005.0	33.54
5.	Lamella5	4	2	14	53717.3	48.69
6.	Lamella6	10	3	8	37005.4	33.54
7.	Lamella7	8	3	12	19055.5	17.27
8.	Lamella8	8	3	16	22087.2	20.02
9.	Lamella9	8	4	8	26705.6	24.21
10.	Lamella10	8	4	12	35135.5	31.85
11.	Lamella11	10	2	8	12339.3	11.18
12.	Lamella12	10	2	12	14724.3	13.35
13.	Lamella13	10	2	16	16271	14.75
14.	Lamella14	10	3	8	15353.2	13.92
15.	Lamella15	10	3	12	19006.8	17.23
16.	Lamella16	10	3	16	21515.7	19.50
17.	Lamella17	10	4	8	17391.4	15.76
18.	Lamella18	10	4	12	22250	20.17
19.	Lamella19	10	4	16	25720.2	23.31
20.	Lamella20	8	2	8	12231.7	11.09
21.	Lamella21	8	2	12	14601.6	13.23
22.	Lamella22	8	2	16	16130.6	14.62
23.	Lamella23	8	3	8	15154.1	13.74
24.	Lamella24	8	3	12	18840.7	17.08
25.	Lamella25	8	3	16	21400.8	19.40
26.	Lamella29	6	2	8	16020	14.52
27.	Lamella30	6	2	12	19071.4	17.29
28.	Lamella31	6	2	16	21015.7	19.05
29.	Lamella32	6	3	8	19925.4	18.06
30.	Lamella33	6	3	12	24613.7	22.31
31.	Lamella34	6	3	16	27923.3	25.31

The results of all examples are elaborated in Table 3 and 4 for limit and ultimate loads and apex displacement corresponding to the limit load, for all the three loading patterns. For reasons mentioned earlier, ultimate load is not obtained for the case of half pressure-half uplift loading and hence are not shown in the table. For Lamella domes having 4 rings, the members do not yield or buckle before the first limit point, and hence the limit points from elastic and inelastic analyses coincide. The values of limit loads in the tables show clearly the conservativeness present in the practice of limit load determination with apex loads only. This is marginally lower for the results of inelastic analysis. The ratio of the limit load predictions is briefly summarized in Table 5. The key point of interest is the near invariance of this ratio for a dome of specific member properties and load distribution pattern. Since the limit loads are the lowest for apex only loading, it is expected that if a greater share of the load is distributed to the rings (from the current 60%), this

ratio would further increase, and vice versa. This has direct implications in design since the apex loading habit in finding limit loads would lead to significant overdesigns.

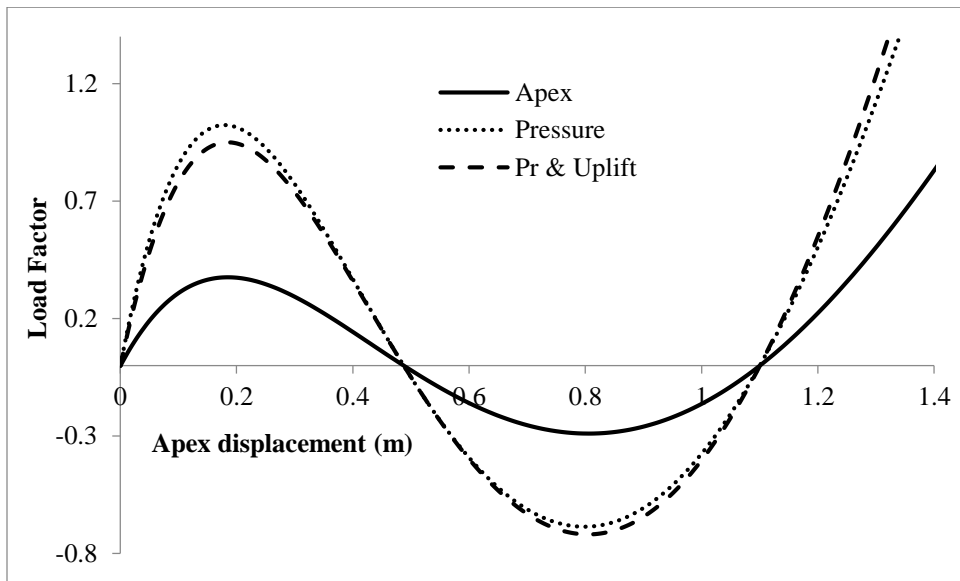


Figure 6: Elastic post-buckling curves for Geodesic 19 dome

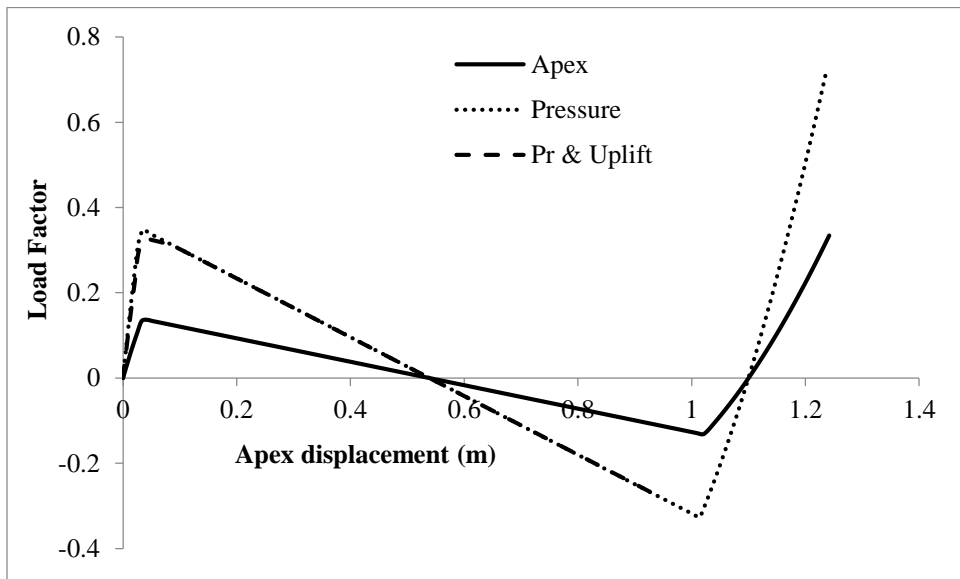


Figure 7: Inelastic post-buckling curves for Geodesic 19 dome

Table 3: Limit and Ultimate loads and apex displacements for selected Geodesic domes (units: kN, m)

Dome <sup>1</sup>	Half Pressure, Half Uplift				Pressure Loading						Apex Loading					
	Elastic		Inelastic		Elastic		Inelastic		Elastic		Inelastic					
	P <sub>lim</sub> <sup>2,3</sup>	δ <sub>lim</sub>	P <sub>lim</sub>	δ <sub>lim</sub>	P <sub>lim</sub>	δ <sub>lim</sub>	P <sub>lim</sub>	δ <sub>lim</sub>	P <sub>ult</sub> <sup>2</sup>	δ <sub>ult</sub>	P <sub>lim</sub>	δ <sub>lim</sub>	P <sub>lim</sub>	δ <sub>lim</sub>	P <sub>ult</sub>	δ <sub>ult</sub>
G11	6.063	0.786	0.110	0.056	6.994	0.758	0.112	0.010	0.085	4.475	2.310	0.785	0.045	0.009	0.047	4.484
G12	7.246	0.745	0.154	0.102	8.950	0.681	0.168	0.010	0.164	4.543	2.776	0.746	0.067	0.008	0.092	4.570
G13	8.029	0.722	0.204	0.219	10.411	0.641	0.224	0.010	0.293	4.632	3.089	0.717	0.089	0.014	0.166	4.686
G14	1.767	0.345	0.137	0.060	1.891	0.348	0.148	0.020	0.122	2.007	0.690	0.360	0.059	0.019	0.058	2.009
G15	2.128	0.336	0.205	0.070	2.344	0.327	0.222	0.019	0.279	2.036	0.835	0.341	0.089	0.018	0.133	2.038
G16	2.363	0.326	0.274	0.062	2.653	0.310	0.295	0.018	0.495	2.067	0.929	0.327	0.117	0.023	0.217	2.056
G17	0.710	0.199	0.164	0.053	0.741	0.194	0.177	0.030	0.180	1.152	0.279	0.200	0.071	0.029	0.081	1.150
G18	0.856	0.191	0.246	0.048	0.908	0.173	0.265	0.028	0.409	1.207	0.338	0.195	0.104	0.036	0.185	1.204
G19	0.951	0.187	0.325	0.045	1.024	0.177	0.348	0.035	0.754	1.247	0.376	0.188	0.137	0.041	0.335	1.242
G20	11.61	0.98	0.13	0.06	13.35	0.93	0.14	0.01	-	-	4.43	0.99	0.05	0.01	-	-
G21	13.89	0.93	0.19	0.12	17.06	0.87	0.20	0.01	-	-	5.32	0.95	0.08	0.01	-	-
G22	15.38	0.90	0.25	0.26	19.80	0.81	0.27	0.01	-	-	5.92	0.92	0.11	0.01	-	-
G23	3.33	0.45	0.17	0.07	3.56	0.44	0.18	0.02	0.15	2.50	1.30	0.45	0.07	0.02	0.07	2.50
G24	4.01	0.43	0.25	0.08	4.41	0.41	0.27	0.02	0.33	2.53	1.57	0.43	0.11	0.02	0.16	2.53
G25	4.45	0.42	0.33	0.06	4.99	0.39	0.36	0.02	0.59	2.55	1.75	0.42	0.14	0.02	0.28	2.56
G26	1.41	0.26	0.20	0.04	1.47	0.25	0.22	0.02	0.22	1.44	0.55	0.26	0.09	0.02	0.10	1.44
G27	1.69	0.24	0.30	0.05	1.80	0.24	0.32	0.03	0.48	1.48	0.67	0.24	0.13	0.03	0.22	1.48
G28	1.88	0.23	0.40	0.04	2.03	0.23	0.43	0.02	0.89	1.52	0.75	0.24	0.17	0.03	0.40	1.52
G29	26.21	0.99	0.26	0.03	29.911	0.976	0.262	0.010	0.237	5.659	10.015	1.023	0.105	0.009	0.132	5.675
G30	31.35	0.96	0.38	0.14	38.076	0.891	0.393	0.010	0.470	5.734	12.040	0.967	0.157	0.008	0.259	5.757
G31	34.73	0.91	0.49	0.23	44.049	0.816	0.525	0.010	0.809	5.770	13.390	0.938	0.210	0.007	0.450	5.825
G32	7.61	0.46	0.35	0.09	8.123	0.454	0.370	0.010	0.341	2.544	2.973	0.463	0.147	0.019	0.160	2.545
G33	9.18	0.43	0.52	0.08	10.077	0.417	0.552	0.019	0.755	2.562	3.599	0.436	0.221	0.017	0.361	2.582
G34	10.18	0.42	0.69	0.05	11.389	0.401	0.736	0.018	1.357	2.591	4.004	0.421	0.293	0.021	0.644	2.591
G35	3.19	0.25	0.46	0.03	3.334	0.261	0.497	0.021	0.568	2.032	1.257	0.257	0.197	0.019	0.217	1.461
G36	3.85	0.25	0.70	0.04	4.096	0.245	0.738	0.028	1.087	1.590	1.520	0.247	0.295	0.027	0.444	1.485
G37	4.27	0.24	0.92	0.04	4.601	0.235	0.982	0.027	1.990	1.549	1.690	0.243	0.389	0.032	0.916	1.677

<sup>1</sup> For convenience, G denotes Geodesic and L denotes Lamella, <sup>2</sup> The subscript lim denotes limit and subscript ult denotes ultimate, <sup>3</sup> values are load factors and not total loads

Table 4: Limit and Ultimate loads and apex displacements for selected Lamella domes (units: kN, m)

<sup>1</sup> Dome	Half Pressure, Half Uplift				Pressure Loading						Apex Loading					
	Elastic		Inelastic		Elastic		Inelastic		<sup>2</sup> P <sub>ult</sub>	$\delta_{ult}$	Elastic		Inelastic		P <sub>ult</sub>	$\delta_{ult}$
	<sup>2,3</sup> P <sub>lim</sub>	$\delta_{lim}$			P <sub>lim</sub>	$\delta_{lim}$	P <sub>lim</sub>	$\delta_{lim}$								
L11	5.933	0.797	0.081	0.182	6.754	0.774	0.094	0.070	0.077	4.534	2.267	0.798	0.037	0.067	0.042	0.542
L12	7.183	0.738	0.125	0.257	8.801	0.702	0.141	0.060	0.165	4.628	2.754	0.750	0.056	0.076	0.094	4.647
L13	7.999	0.724	0.164	0.198	10.311	0.648	0.185	0.093	-	-	3.076	0.723	0.073	0.092	-	-
L14	1.732	0.376	0.115	0.153	1.803	0.382	0.124	0.167	0.154	2.240	0.683	0.381	0.049	0.169	0.070	2.240
L15	2.077	0.353	0.164	0.198	2.230	0.344	0.178	0.181	0.346	2.433	0.830	0.354	0.069	0.202	0.162	2.452
L16	2.316	0.332	0.205	0.220	2.516	0.322	0.225	0.206	0.654	2.708	0.926	0.339	0.085	0.232	0.322	2.962
L17	0.692	0.214	0.069	0.214	0.710	0.220	0.071	0.220	0.235	1.542	0.277	0.216	0.028	0.216	0.110	1.557
L18	0.841	0.202	0.084	0.202	0.871	0.198	0.087	0.198	0.572	1.897	0.337	0.195	0.034	0.195	0.249	2.182
L19	0.938	0.185	0.094	0.185	0.976	0.190	0.098	0.190	0.668	1.950	0.375	0.188	0.038	0.188	0.290	1.957
L20	10.926	1.020	0.108	0.212	12.896	0.997	0.114	0.050	0.094	5.650	4.347	1.024	0.046	0.057	0.050	5.655
L21	13.769	0.946	0.152	0.266	16.779	0.894	0.172	0.049	0.200	5.726	5.283	0.963	0.068	0.059	0.112	5.742
L22	15.310	0.915	0.201	0.180	19.610	0.827	0.229	0.049	0.371	5.856	5.896	0.911	0.090	0.066	0.206	5.867
L23	3.266	0.472	0.148	0.146	3.398	0.480	0.160	0.128	0.180	2.693	1.289	0.469	0.063	0.129	0.081	2.694
L24	3.915	0.441	0.217	0.154	4.200	0.427	0.235	0.135	0.430	2.961	1.565	0.435	0.092	0.148	0.196	2.946
L25	4.366	0.419	0.281	0.180	4.736	0.407	0.304	0.158	0.767	3.150	1.746	0.422	0.119	0.174	0.350	3.138
L29	24.731	1.043	0.238	0.213	28.925	1.021	0.253	0.049	0.213	5.712	9.843	1.029	0.101	0.057	0.113	5.714
L30	31.096	0.955	0.340	0.245	37.475	0.915	0.379	0.049	0.478	5.799	11.951	0.983	0.151	0.058	0.260	5.808
L31	34.582	0.918	0.448	0.177	43.638	0.851	0.506	0.048	0.830	5.908	13.335	0.927	0.200	0.065	0.458	5.920
L32	7.460	0.481	0.331	0.148	7.755	0.488	0.355	0.127	0.410	2.735	2.944	0.477	0.141	0.129	0.184	2.736
L33	8.957	0.447	0.485	0.157	9.597	0.444	0.522	0.136	0.903	2.895	3.581	0.452	0.205	0.147	0.417	2.907
L34	9.908	0.475	0.627	0.187	10.817	0.415	0.678	0.154	1.715	3.158	3.992	0.428	0.265	0.173	0.780	3.219

<sup>1</sup> For convenience, G denotes Geodesic and L denotes Lamella, <sup>2</sup> The subscript lim denotes limit and subscript ult denotes ultimate, <sup>3</sup> values are load factors and not total loads

Table 5: Ratio of limit and ultimate load predictions of distributed loading to predictions of apex loading

Ratio	Geodesic Type			Lamella Type		
	Maximum	Minimum	Average	Maximum	Minimum	Average
Limit load: Pressure loading to half pressure-half uplift	1.30	1.04	1.13	1.29	1.03	1.14
Limit load: Pressure loading to apex loading	3.37	2.65	2.89	3.35	2.63	2.91
Ultimate load: Pressure loading to apex loading	2.54	2.49	2.50	2.63	2.5	2.54

### 3.4 Influence of number of rings

The number of rings appear to have contradictory effects in elastic analysis and inelastic analysis. The limit load undergoes clear reductions with greater number of rings in case of elastic analysis. There is however steady increase in limit loads with increasing number of rings in the case of inelastic analysis. The reason for the latter is obvious given that greater number of rings leads to more members in the dome, more redistribution, and consequently lower member forces. This delays the load factor at which member buckling or yielding occurs, thus increasing the limit load.

For the adverse effect of rings on elastic analysis, the explanation is based on a ‘zonal’ effect. With a fixed span/rise ratio, when the number of rings is greater, the zone undergoing snap-through is closer to the top and hence shallower, causing a reduction in the limit loads. These points are illustrated in Figs 8-10. Fig 8 in particular shows that it is indeed the member forces of the members confined in this zone that causes the occurrence of the limit point. Similar trends according to the number of rings is seen also with inelastic analysis.

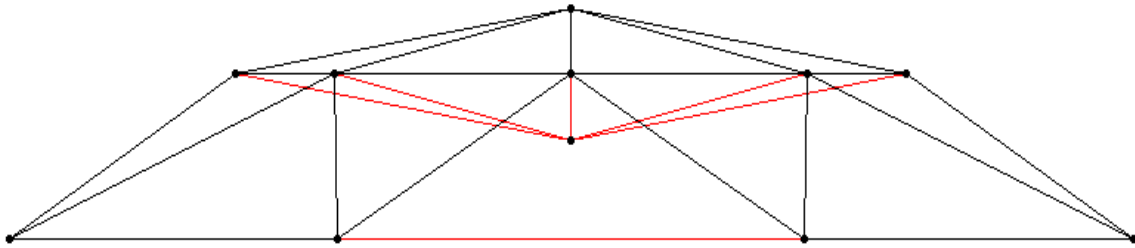


Figure 8: Snap-through occurring in the confined part of the uppermost ring

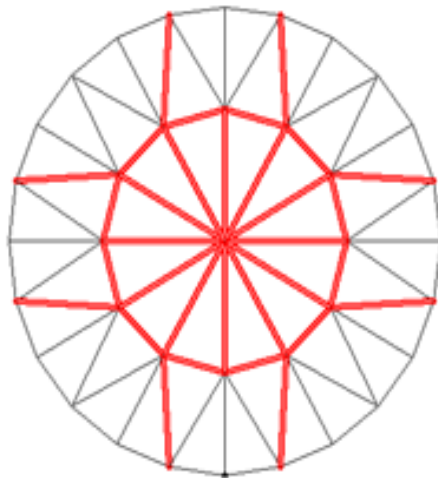


Figure 8: Critical members of a geodesic type dome under pressure loading

Figs 9-10 shows the effect of number of rings for rise-span ratio 10, for varying number of members at the apex. The figures are shown for pressure loading but the same trend was observed for all loading patterns.

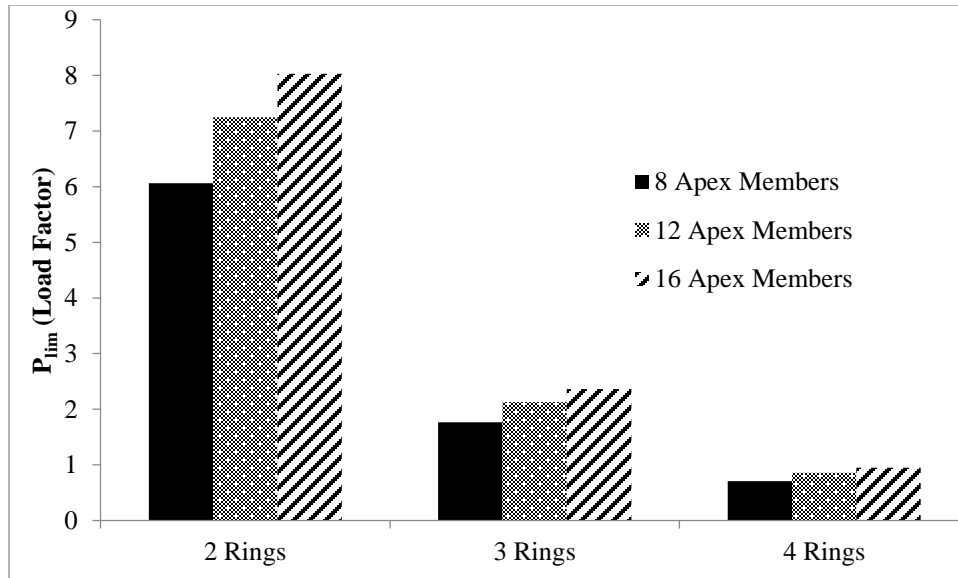


Figure 9: Variation of limit loads with number of rings (Elastic analysis)

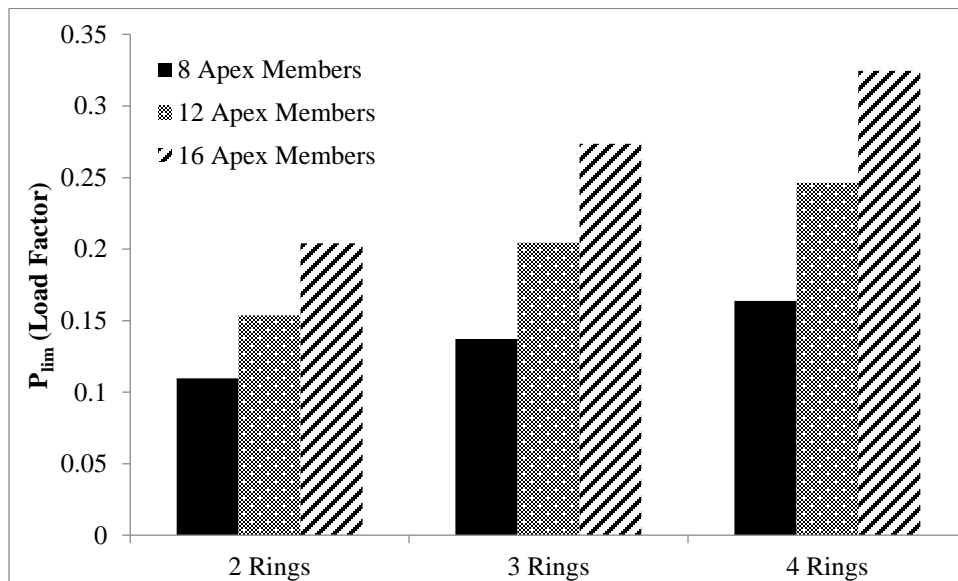


Figure 10: Variation of limit loads with number of rings (Inelastic analysis)

However, the percentage increase in the limit load is practically constant as the number of members is increased from 8 to 12 and from 12 to 16. This is true irrespective of the span-rise ratio, the number of rings and even the loading distribution pattern. Typical percentage of increase is listed in Table 6. Clearly, in inelastic analysis the percentage increase in the limit loads is almost equal to the percentage increase in the number of members. However, for elastic analysis, in which the limit point is not caused by member effects (buckling or yielding) the percentage increase is not correlatable to the number of members. It is to be remembered however that, the limit loads from inelastic analysis would be definitely much lower than that from elastic analysis, for a given number of rings.

Table 6: Effect of number of members at apex on limit loads

Members at apex increase from	Geodesic			Lamella		
	Half pressure – half uplift	Pressure Loading	Apex Loading	Half pressure – half uplift	Pressure Loading	Apex Loading
Elastic Analysis: 8 to 12	20%	25%	20%	23%	25%	22%
Elastic Analysis: 12 to 16	11%	13%	11%	11%	14%	12%
Inelastic Analysis: 8 to 12	49%	49%	50%	45%	50%	49%
Inelastic Analysis: 12 to 16	32%	33%	32%	32%	32%	33%

#### 4. Comparison of results with approximate closed-form expression – Wright’s formula and generation of predictor equation

The Wrights formula, given by Eq 8, is compared with the limit load predictions obtained by the procedure in this study. It is to be noted that Wright’s formula given the critical loads  $q_{cr}$  in terms of pressures (kN/m<sup>2</sup>) and therefore the limit loads obtained in this study are divided by the plan area of the dome in order to make a comparison.

$$\frac{AEI}{12R^3} < q_{cr} < \frac{AEI}{6R^3} \quad (8)$$

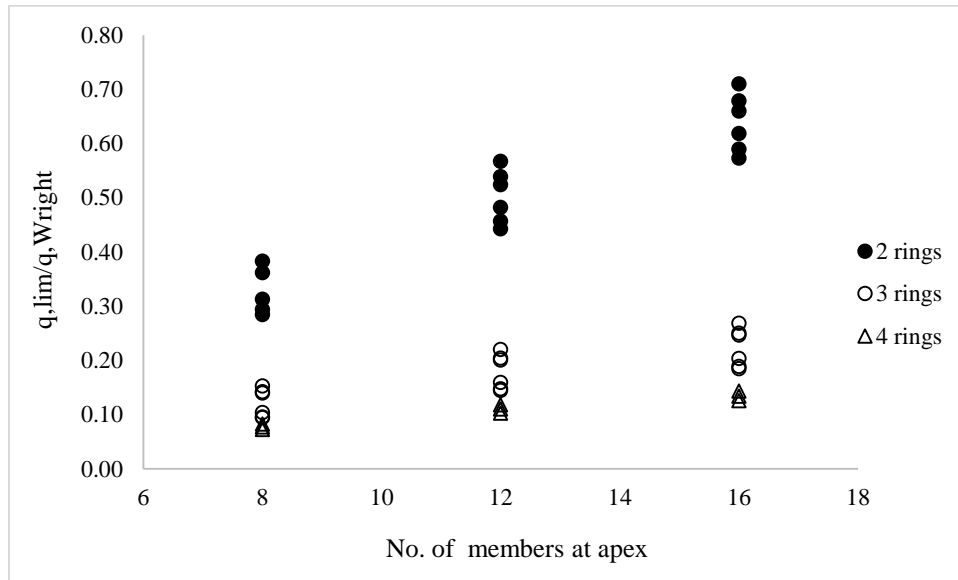


Figure 11: Scatter of ratio of limit loads (study) to Wright’s formula limit loads

In the formula  $R$  is the spherical radius of the dome. Fig 9 shows that the deviation with Wright’s formula is higher for domes with greater number of rings with a specific number of apex members. The formula is also seen to gain accuracy as the number of apex members increases. The ratio of the obtained in the study to that given by the lower limit of Wright’s formula is about 0.7 for 16 members at the apex and two rings. Given that this ratio is itself with respect to the formula’s lower bound, it can be stated that the Wright’s formula is unconservative for predictions of the elastic limit load. Most closed form expressions do not relate to member effects such as buckling or yielding in their formulae and hence similar comparisons cannot be made for inelastic limit loads.

To address this gap in unavailability of prediction expressions, it was sought to carry out a regression on the generated results of both types of domes. Since the two types of domes differ in geometry, they were considered separately for the regression. Initially nonlinear regression of the form shown in Eq. 9 (Dara, 2019) was attempted but the predictions were extremely unsatisfactory. Hence, as an preliminary step, linear regression was performed for prediction equations for limit loads for all 3 loading cases and ultimate loads for pressure and apex only loading cases. The input parameters chosen were the span-rise ratio, number of rings, number of members at the apex and the average length (in terms of  $EI/L_{avg}$ ). The axial rigidity was omitted, since the ultimate loads in most examples were reached by member buckling rather than yielding. Table 7 below shows the regression coefficients for the parameters and the  $R^2$  value for each equation generated. For the equations generated for ultimate loads, span-rise ratio was omitted since the P-value was high ( $>0.5$ ) and the regression was performed again to get the coefficients in Table 7.

Table 7: Coefficients of regression for prediction of limit and ultimate loads

Dome Geometry	Case <sup>1</sup>	Regression coefficient for parameter					Adjusted $R^2$
		Span/rise	No. of rings	No. of members at apex	$\frac{EI}{L_{avg}^2}$	Intercept	
Geodesic	Limit load: Half pressure-half uplift	-3.485	-12.747	0.738	13.471	55.744	0.9704
	Limit load: Pressure	-3.651	-13.240	0.856	14.228	57.379	0.9674
	Limit load: Apex load	-1.477	-5.256	0.344	5.623	23.066	0.9668
	Ultimate load: Pressure	-	-31.735	3.039	34.124	22.192	0.9190
	Ultimate load: Apex load	-	-16.285	1.658	15.272	14.048	0.8816
Lamella	Limit load: Half pressure-half uplift	-4.193	-8.074	-0.373	21.151	58.262	0.8585
	Limit load: Pressure	-4.591	-9.084	-0.262	22.344	63.627	0.8543
	Limit load: Apex load	-1.852	-3.500	-0.104	8.632	25.531	0.8574
	Ultimate load: Pressure	-	-16.386	0.279	74.062	0.577	0.8853
	Ultimate load: Apex load	-	-9.332	0.416	33.232	3.741	0.8778

<sup>1</sup> All output loads fitted in kN for total of all loads acting on the dome

It is seen that the coefficients obtained are satisfactory with adjusted  $R^2$  values greater than 0.95 for the Geodesic Type domes. The usage of the same parameters however is unsatisfactory for Lamella type domes having adjusted  $R^2$  values lesser than 0.9. A few of the Lamella domes did not undergo member buckling even while performing inelastic analysis and this could be cited as a possible reason for the relatively poor performance of the regression with same parameters.

## 5. Conclusions

This study demonstrates the post-buckling behavior of single layer reticulated shells with loads acting on the ring nodes rather than just the apex. The basis of the nonlinear formulation, the corotated-updated Lagrangian formulation was summarized, along with the methods for incorporation of member inelasticity and buckling. A total of 67 domes – in Geodesic and Lamella type geometries were run through elastic and inelastic post-buckling analyses for three loading distributions namely apex loading, distributed pressure (downward) loading and half pressure-half uplift loading. The limit loads, ultimate loads and corresponding displacements obtained through the analyses give some valuable information on the effect of distributed loading on the postbuckling behavior. The results were also compared with the popular Wright’s formula for

assessing the suitability of the expression. Some of the conclusions that can be stated based on the results of the study are listed below:

- a. The distribution of load on the dome surface enhances the global buckling capacity (i.e. raises the limit load) of single layer domes. This is true with both elastic and inelastic analyses. While elastic limit load predictions with distributed loading are upto 2.9 times the elastic limit loads with apex loading, for inelastic limit loads, this ratio is about 2.5
- b. The ratios above are dependent on the proportion of the total loads on the ring. The lowest loads are when the dome is loaded at only the apex, and when the load is distributed perfectly on all nodes, the ratio is expected to be the highest.
- c. Domes with more number of rings are susceptible to snap-through as long as the individual members are within their yield and buckling limits. But in the scenario of members exceeding these limits (inelastic postbuckling analysis of the dome), the more the rings, the higher is the limit load of the structure. This is due to a greater number of members in the structure, which eases the forces carried by each member, thus delaying the limit point. Thus the number of rings is an important parameter in design, which should be taken into account while simultaneously keeping elastic and inelastic limit loads above the required values.
- d. The lower bound of the closed-form Wright's formula for elastic limit loads (in terms of pressure) is unconservative for single layer domes. The unconservativeness is greater for higher number of rings and members at the apex.
- e. Linear regression was performed for Geodesic and Lamella domes in the search of a prediction equation for the limit and ultimate loads with consideration of inelastic behavior. While the expression is satisfactory for Geodesic domes within the range of values in this study, the same confidence is not obtained for Lamella type domes. However, this serves as a starting point towards formulating more acceptable prediction equations for the limit and ultimate loads of single layer domes.

This study can be extended further to include more dome geometries, load distributions and dome dimensions. Additionally, the effect of joint flexibility, which is reported in literature to have profound bearing on limit loads, can also be taken into consideration.

## References

- Ahmadizadeh, M and Maleek, S. (2014). "An investigation of the effects of socket joint flexibility in space structures." *Journal of Constructional Steel Research*, 102, 72-81.
- Argyris, J.H. (1982). "Finite element analysis of two and three dimensional elasto plastic frames – the natural approach." *Computational Methods in Applied Engineering*, 35, 221-248.
- Axelsson, K., and Samuelsson, A. (1979). "Finite element analysis of elastic-plastic materials displaying mixed hardening." *International Journal for Numerical Methods in Engineering*, 14(2), 211-225.
- Belytschko, T. and Hsieh, B.J. (1973). "Nonlinear transient finite element analysis with convected co-ordinates." *International Journal for Numerical Methods in Engineering*, 7(3), 255-271.
- Bergan, P.G. and Soreide, T.H. (1978). "Solution of large displacement and instability problems using current stiffness parameter." *Finite elements in nonlinear mechanics*, (Eds.) P.G. Bergan et al, Tapir, Trondheim, 647-669
- Bhatti, M.A. (2006). "Fundamental finite element analysis and applications: with Mathematica and Matlab computations." John Wiley & Sons, 2006
- Chan, S.L. (1988). "Geometric and material non-linear analysis of beam-columns and frames using the minimum residual displacement method." *International Journal for Numerical Methods in Engineering*, 26, 2657-2669
- Crisfield, M.A. (1981). "A fast incremental/iterative solution procedure that handles snap-through". *Computers & Structures*, 13, 55-62.

- Dara, P. (2019). "Postbuckling Strength of Single Layer Domes under Distributed Loading." Masters Dissertation, National Institute of Technology Tiruchirappalli, India.
- Guo, X., Xiong, Z., Luo, Y., Qiu, L., and Liu, J. (2015). "Experimental investigation on the semi-rigid behavior of aluminium alloy gusset joints." *Thin-walled Structures*, 87, 30-40.
- Han, Q., Liu, M., and Xu, Y. (2016). "Stiffness characteristics of joints and influence on the stability of single-layer latticed domes." *Thin-walled Structures*, 107, 514-525.
- Hill, C.D., Blandford, G.E., and Wang, S.T. (1989). "Post-buckling analysis of steel space trusses." *Journal of Structural Engineering, ASCE*, 115(4), 900-919.
- Jayachandran, S.A., Kalyanaraman, V., and Narayanan, R. (2004). "A co-rotation based secant matrix procedure for elastic postbuckling analysis of truss structures." *International Journal of Structural Stability and Dynamics*, 4(1), 1-19.
- Lopez, A., Puente, I., and Serna, M.A. (2007). "Numerical model and experimental tests on single-layer latticed domes with semi-rigid joints." *Computers & Structures*, 85, 360-374.
- Ma, H., Fan, F., Wen, P., Zhang, H., and Shen, S. (2015). Experimental and numerical studies on a single-layer cylindrical reticulated shell with semi-rigid joints." *Thin-Walled Structures*, 86, 1-9.
- Papadrakakis, M. (1983). "Inelastic post-buckling analysis of trusses." *Journal of Structural Engineering, ASCE*, 109(9), 2129-2147.
- Saitoh, M., Hangai, Y., Toda, I., Yamagiwa, T., and Okuhara, T. (1986). "Buckling loads of reticulated single-layer domes." *Proceedings of the IASS symposium, vol. 3, Osaka*, , 121-128
- Thai, H.T. and Kim, S.E. (2009). "Large deflection inelastic analysis of space trusses using generalized displacement control method." *Journal of Constructional Steel Research*, 65, 1987-1994.
- Wright, D.T. (1965). "Membrane Forces and Buckling in Reticulated Shells." *Journal of the Structural Division, ASCE*, 91(1), 173-202.
- Xiong, Z., Guo, X., Luo, Y., Zhu, S., and Liu, Y. (2017). " Experimental and numerical studies on single-layer reticulated shells with aluminium alloy gusset joints." *Thin-walled Structures*, 118, 124-136.
- Yang, Y.B., Yang, C.T., Chang, T.P., and Chang, P.K. (1997). Effects of member buckling and yielding on ultimate strengths of space trusses." *Engineering Structures*, 19(2), 179-191.